2016-12

Integrated Design of Downwind Land-based Wind Turbines using Analytic Gradients

Andrew Ning
Brigham Young University, aning@byu.edu

Derek Petch
National Renewable Energy Laboratory

RESEARCH ARTICLE

Integrated Design of Downwind Land-based Wind Turbines using Analytic Gradients

Andrew Ning[1] and Derek Petch[2]

[1] Brigham Young University, Provo, UT, 84602
[2] National Renewable Energy Laboratory, Golden, CO, 80401

ABSTRACT

Wind turbines are complex systems where component-level changes can have significant system-level effects. Effective wind turbine optimization generally requires an integrated analysis approach with a large number of design variables. Optimizing across large variable sets is orders of magnitude more efficient with gradient-based methods as compared to gradient-free method, particularly when using exact gradients. We have developed a wind turbine analysis set of over 100 components where 90% of the models provide numerically exact gradients through symbolic differentiation, automatic differentiation, and adjoint methods. This framework is applied to a specific design study focused on downwind land-based wind turbines.

Downwind machines are of potential interest for large wind turbines where the blades are often constrained by the stiffness required to prevent a tower strike. The mass of these rotor blades may be reduced by utilizing a downwind configuration where the constraints on tower strike are less restrictive. The large turbines of this study range in power rating from 5–7 MW and in diameter from 105–175 m. The changes in blade mass and power production have important effects on the rest of the system and thus the nacelle and tower systems are also optimized. For high-speed wind sites, downwind configurations do not appear advantageous. The decrease in blade mass (10%) is offset by increases in tower mass caused by the bending moment from the rotor-nacelle-assembly. For low-wind speed sites the decrease in blade mass is more significant (25–30%) and shows potential for modest decreases in overall cost of energy (around 1–2%).

Correspondence

Andrew Ning, BYU, 435 CTB, Provo, UT 84602.

E-mail: aning@byu.edu

NOMENCLATURE

AEP	annual energy production
COE	cost of energy
D	rotor diameter
H	tower height
V_{rated}	rated speed
Ω	rotor rotational speed or frequency
δ	deflection
ϵ	strain
η	safety factor
σ	standard deviation
σ_{VM}	von Mises stress
σ_y	yield stress
θ	blade twist
c	chord
d	diameter
f	frequency
t	thickness

x precurve

1. INTRODUCTION

Reducing the cost of energy of wind turbines requires a careful balance of energy production with capital investment, operational, and maintenance costs. Because of the multidisciplinary trade-offs, assessment of alternative technologies requires an integrated design process. Currently, most design studies focus on the design of a single component such as rotor design, or foundation design. A few studies explore holistic turbine design [1, 2], but because of the complexity and longer simulation times, these type of studies appear less frequently and rely on simplified scaling methods or metamodels. This work examines an efficient approach to integrated, physics-based turbine optimization enabled by analytic gradients.

One of the major barriers to efficient integrated design is that most simulation tools were developed for analysis purposes and not for the needs of optimization. As a result, many analysis tools produce output that is non-differentiable, or do not always converge. This type of function behavior forces the user towards gradient-free optimization methods. Gradient-free methods are robust because they do not require differentiability, can tolerate occasional solution failures, and are easily coupled with existing analysis tools. However, the major limitation of gradient-free methods is that they do not scale well to large numbers of design variables. Figure 1 for example, shows the number of function evaluations required for convergence as a function of problem dimensionality (the number of design variables). This figure was generated with the multidimensional generalization of the Rosenbrock function, but similar trends have been observed using 3D Navier-Stokes aerodynamic shape optimization [3]. As the number of design variables increases, gradient-free methods quickly become intractable. When designing a single wind turbine component, one can generally achieve sufficient resolution with a small number of design variables. However, as the focus moves from component design to integrated turbine or wind farm design, the number of design variables will of necessity increase and gradient-based methods, particularly those that can supply exact gradients, will be come increasingly critical.
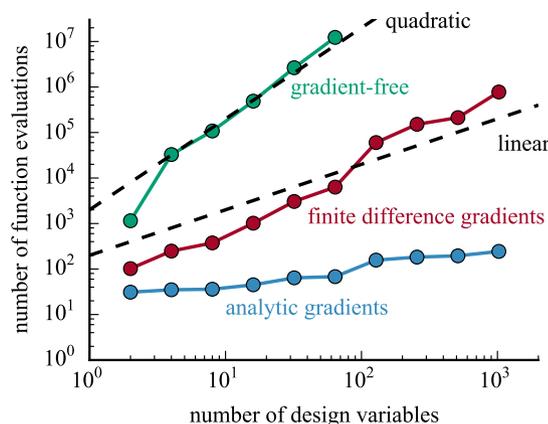

Figure 1. Number of function evaluations required to converge optimization as a function of number of design variables. Sparse Nonlinear OPTimizer was used for the gradient-based results and Augmented Lagrangian Particle Swarm Optimizer for the gradient-free results, however similar trends were observed using Sequential Least SQuares Programming (gradient-based) and Non Sorting Genetic Algorithm II (gradient-free). Reference lines for linear and quadratic scaling are also shown.

As suggested by Fig. 1, gradient-based methods with finite differencing are a significant improvement over gradient-free methods. Generally some work is needed to modify the analysis tools to ensure differentiability under all conditions (smoothing out empirical correction factors, tightening convergence loops, etc.). The actual computation of gradients through finite differencing is extremely simple to apply and most optimization tools have this capability built in. However, the number of function calls required to compute finite-difference gradients scales at least linearly with the number of design variables and can quickly become a computational bottleneck. Our recent study on wind plant layout optimization contained around 4,000 design variables and exemplified the scaling difficulty of finite differencing [4]. Furthermore, the accuracy of finite-difference gradients is limited (generally to 6 significant figures or less), which can cause issues with convergence. Using a very similar setup to that described in this paper, we found that finite-differencing led to inferior solutions and in many cases failed to converge at all [5].

The ideal scenario for design optimization purposes is to provide analytic gradients and this has been one of the major focuses of our development effort. We have developed a set of methods and tools that are not only differentiable, but

in almost all cases provide analytic gradients through the use of adjoint methods, automatic differentiation, and in some cases symbolic derivation.[*] Obtaining analytic derivatives is far more complicated than using finite-differencing because it is intrusive into the specific algorithms. However, as seen in Fig. 1 the pay-off is significant especially as we move into problems with larger numbers of design variables. The power of adjoint methods and analytic gradients has grown in recognition and capability over the last decade. Its use is still emerging even in aerospace applications; to the best of our knowledge this is the first use of analytic gradients across more than one component for wind turbine applications.

In this paper we apply these methodologies to a specific study comparing downwind turbines to upwind turbines using a moderate number of design variables, but a very large number of integrated components. Downwind turbines have grown in interest as advances in materials and structural design have enabled taller towers and larger rotors for utility-scale turbines. Larger turbines can produce more power because of the larger swept area of the rotors and the faster wind speeds at higher hub heights. However other design constraints make larger blades increasingly challenging. In the worst-case operating conditions, the blades must be stiff enough to not strike the tower. For upwind cantilevered blades, achieving adequate blade stiffness requires large structural mass, the cost of which may offset any gains in energy production. One potential avenue to reduce the required blade stiffness is to switch from a traditionally-used upwind configuration to a downwind one.

Downwind turbines are less restricted by tower-strike, and from a stiffness standpoint are constrained primarily by frequency response and buckling constraints. Increased fatigue damage from the tower shadow becomes a concern, but may be alleviated through aerodynamic fairing on the tower or other means [6]. A recent study by Reiso on downwind turbines suggested that blade mass could be reduced by 20% with a corresponding 5% reduction in blade fatigue loads without sacrificing power [7]. This study found that benefits to the blades came at the expense of a 20% larger tower bottom bending moment, although no assessment was made on the corresponding impact to the tower mass or system costs. They also showed that while even more flexible blades were feasible, they led to decreases in power production. Other system benefits of downwind turbines have been suggested in the literature. A wind plant study by Yoshida suggested that downwind turbines would be beneficial in complex terrain because the terrain topology often induces an upward flow and the tilt of downwind turbines is much closer to perpendicular to the incoming wind [8]. Reiso and Moe [9] discuss how downwind turbines enable simpler yaw systems, which can lead to significant maintenance cost reductions, especially offshore.

This study is concerned with comparing large land-based upwind and downwind rotors using the same design criteria to estimate the potential system benefits of downwind configurations. Nonlinear optimization and design criteria, primarily that of the International Electrotechnical Commission (IEC) [10], are used to size the turbines. We should emphasize that our goal is not to design a downwind machine, or to provide accurate cost estimates. Instead, we seek to understand fundamental system-level trade-offs in upwind and downwind machines using a methodology that allows us to fully converge and compare solutions using a highly multidisciplinary physics-based analysis.

2. METHODOLOGY

The design methodology extends that described previously by Ning [11], but with much more detailed tower modeling, a new drivetrain model, a larger number of design variables, and improved and expanded constraint handling. The previous methodology was rotor-centric, but the new methods allow for physics-based sizing of the nacelle assembly and the tower. Some of these additions are described in a recent study on high tip-speed rotors [12]; additional improvements in supplying gradients and in modeling curved or highly flexible blades are discussed below. Table I summarizes the methodology used for the physics-based portions of the analysis; additional detail is provided by Ning [11, 12] and in the following subsections.

The rotor and tower models are physics-based models with dimensions sized using nonlinear optimization. The new drivetrain model is no longer based solely on scaling, but instead performs a physics-based sizing of the bedplate, low- and high-speed shaft, main and secondary bearings, gearbox, yaw system, and transformer.[†] Even though the rotor was the most affected component, including the nacelle and tower in the optimization process was important to capture system-level impacts.

The blade geometry and thickness of the laminate stacks were optimized for the various rotor designs, but the laminate schedules were kept constant. Laminate schedule optimization involves a large number of discrete variables, and the additional complexity was unwarranted for the purposes of this study. The laminate schedule used in this study came from Sandia National Laboratory and was designed to approximately match the structural distributions specified by the NREL 5-MW reference model, while simultaneously satisfying IEC load requirements [13]. The total thickness of the spar-cap

---

[*] These tools have also been open-sourced and are available at `www.github.com/WISDEM`.

[†] `https://github.com/WISDEM/DriveSE`

Table I. Wind turbine analysis methods.

Discipline	Theories	Codes
Blade aerodynamics	Blade element momentum	RotorSE, CCBlade
Blade structures	Beam finite element, classical laminate theory	RotorSE, pBEAM
		CurveFEM, PreComp
Tower aerodynamics	Power-law wind profile, cylinder drag	TowerSE
Tower structures	Beam finite element, Eurocode, Germanischer Lloyd	TowerSE, pBEAM
Nacelle sizing and structures	Mechanical design	DriveSE

and aft-panel laminates were sized directly by the optimization, while leading-edge panels and shear webs were indirectly sized relative to the section thickness. Airfoil profiles (for unit chord) were also fixed to avoid additional complexity and uncertainty in the estimation of aerodynamic performance of very thick sections.

Turbine capital costs were estimated using recently developed mass-based cost models[‡]. This model is a significant improvement compared to the previous cost and scaling model. Rather than simply scale costs based on macro turbine parameters like rotor diameter, the capital cost model is based on the mass of individual components (e.g., blades, hub, bedplate, low-speed shaft, etc.). This is important in these conceptual studies where macro parameters may be fixed while detailed blade and tower shapes are modified. Balance-of-station costs are estimated using a recently developed bottom-up model for land-based turbines[§]. The balance of station model no longer uses simple scaling, but rather bottom-up estimates of all the contributions to total balance of station costs (e.g., transportation, engineering, access roads, project management, insurance, etc.). Operations and maintenance costs came from the NREL cost and scaling model [14].

2.1. Rotor Analysis

The rotor analysis was based on steady aeroelastic loading primarily using blade element momentum theory, classical laminate theory, and beam finite element theory. The blade element momentum theory was based on a new solution methodology [15] that has guaranteed convergence; this functionailty is critical for gradient-based optimization. Additionally, analytic gradients were provided for all outputs using automatic differentiation and an adjoint method.

The study by Resor [13] was used to validate and in some cases calibrate the various design constraints for the baseline NREL 5-MW design. Resor's work was also helpful in selecting which of the IEC design load cases (DLC) were likely to be most critical for this study. Because of the large number of components integrated in this study, a full IEC loads analysis was not computationally feasible, so a select number of DLCs were preselected based on Resor's analysis. The aerodynamic and structural models, DLCs, constraints, and unique considerations for downwind rotors are discussed in the following sections.

2.1.1. Power Production

Flexible blades can undergo significant deflection under load. This out-of-plane blade bending involves a coupling between the aerodynamic loading and the structural deformation. If the downwind deflection of the blade is not considered when generating power curves, then the AEP is often overpredicted. The coupled aero/structural solution of the deflected blade shape was found using an internal fixed point iterator between the blade aerodynamics and structural analyses converged to a tolerance of 1×10^{-8}, repeated at every analysis iteration. An adjoint method was used around this solver to compute coupled gradients.

For the purposes of estimating AEP, recomputing the blade deflection at every point along the power curve would have tremendously increased computational time. AEP was computed for several configurations with the aerodynamics and structures fully coupled throughout the power curve, and the results were compared to AEP predictions where the deflection from one wind speed was used throughout the power curve. For each configuration, the annual energy production was found to best agree by using the deflection for a wind speed between 65–75% of the rated speed. For all AEP calculations, the out-of-plane structural deformation of the blade at 70% of the rated speed was used throughout the power curve. For upwind rotors, including the downwind structural deflection in the power calculation had a negligible impact because of the high stiffness. However, for downwind designs the potential for significantly decreased blade stiffness is high, and capturing this trade-off in power production loss was a critical consideration.

2.1.2. Tower and Ground Strike

The maximum out-of-plane tip deflection was constrained to avoid tower strike for upwind configurations. The study by Resor [13] found that the maximum out-of-plane deflection for this blade occurred at IEC DLC 1.3 extreme turbulence model (ETM).[¶] The out-of-plane blade tip deflection is maximum near rated speed. Tip deflection was estimated at $180°$ azimuth with the nominal wind speed at V_{rated} with a 3σ gust. The standard deviation for the turbulence was estimated from the ETM for a "category B" level of turbulence. Because the deflection is computed under static loading, a calibration factor for dynamics was added. Both the studies by Jonkman [16] and Resor [13] used NREL's aeroelastics code FAST and estimated the maximum out-of-plane tip deflection for this blade to be around 5.6 m. The tip deflection computed from the static analysis was multiplied by 1.2 to correct for the dynamic effects and yields a tip deflection that agrees with that of the previously published studies to within less than 1%. The curvature of the blades was accounted for in the coordinate transformation to the tower coordinate system for both the total loads (aerodynamic + inertial + centrifugal) and the tip deflection.

The allowable deflection was a function of the blade length, curvature, precone and tilt angles, and the tower dimensions. The available clearance was reduced using a total safety factor of $\eta_{dfl} = 1.485$ (1.35 loads, 1.1 materials, and 1.0 consequences of failure). The resultant constraint was imposed as:

$$\delta_{tip}\,\eta_{dfl} \leq \delta_{max} \tag{1}$$

Similarly, the clearance between the ground and the blade tip was computed and constrained to be at least 20 m. Local ordinances have significant variability in minimum ground clearance requirements, but for this study it was never an active constraint anyway.

$$\delta_{ground} \geq 20 \tag{2}$$

2.1.3. Natural Frequencies

In order to estimate natural frequencies for curved blades, the existing code CurveFEM [17] was incorporated into the analysis. CurveFEM was designed to compute natural frequencies for blades with precurve and presweep. The estimated natural frequencies for the baseline design agree to within less than 10% of those from the previous published studies on the NREL 5-MW reference model [13, 16] (with the frequencies in this study erring on the side of conservatism). The first flapwise mode (and consequentially all modes) was constrained to be 10% larger than the maximum blade passing frequency.

$$f_0 \geq 1.1\,n_{blades}\Omega_{rated} \tag{3}$$

2.1.4. Ultimate Strength

Axial strain was computed under a combined loading condition with a 50-year survival wind at $90°$ to the pitch axis and the blade in the 12 o'clock position (approximately the worst-case loading condition for this blade). Strain was computed at the outer edge of the airfoil in the midpoint of the panel for both the spar-cap panels and the trailing-edge panels. The strain at each section was multiplied by the safety factor $\eta_{str} = 1.755$ (1.35 loads, 1.3 materials, and 1.0 consequence of failure). For the spar cap it was assumed that the ultimate strain was 10,000 microstrain in both tension and compression, which is a representative conservative value for the materials used in the blade. For the trailing-edge panels the maximum strain was assumed to be 2,500 microstrain per GL guidelines [18]. The Sandia study also found IEC DLC 6.1 extreme wind speed model to be the critical ultimate strain condition. While they did not do a combined load case, the magnitudes of the worst-case conditions agree to within less than 5% (again with these results erring on the side of conservatism).

The constraint is only applied at a subset of the stations. Because the strain varies smoothly, this allows the number of constraints to be reduced without affecting the solution (an assumption which is always checked for any optimized solutions). The constraint is applied as

$$-\epsilon_{ult} \leq \epsilon\,\eta_{str} \leq \epsilon_{ult} \tag{4}$$

2.1.5. Panel Buckling

The constitutive equations for a laminate sequence can be expressed as

$$\left[\begin{array}{c} N \\ \hline M \end{array}\right] = \left[\begin{array}{c|c} A & B \\ \hline B & D \end{array}\right] \left[\begin{array}{c} \epsilon^0 \\ \hline k \end{array}\right] \tag{5}$$

[¶]The study actually showed DLC 1.4 extreme direction change (EDC) as the condition producing the largest deflection, however only a PI controller was used for speed regulation and no controller logic was asserted for start-up and shutdowns. The controller response to ECD, had there been one, would have substantially reduced turbine loads and resulted in turbine shutdown in the event of an extreme direction change.

where N and M are the average forces and moments of the laminate per unit length, and ϵ^0 and k are the mid-plane strains and curvature (see [19]). The D matrix is a 3×3 matrix of the form[||]

$$
\begin{bmatrix}
D_{11} & D_{12} & 0 \\
D_{12} & D_{22} & 0 \\
0 & 0 & D_{66}
\end{bmatrix}
\tag{6}
$$

The critical buckling load for long (length greater than twice the width) simply supported panels at a given section is estimated as (see [20]):

$$
N_{cr} = 2 \left(\frac{\pi}{w}\right)^2 \left[\sqrt{D_{11}D_{22}} + D_{12} + 2D_{66}\right]
\tag{7}
$$

where w is the panel width. The critical strain is then

$$
\epsilon_b = -\frac{N_{cr}}{T\ E}
\tag{8}
$$

where T is the total thickness of the laminate stack, E is the effective axial modulus of elasticity for the stack, and the negative sign accounts for the fact that the strain is compressive in buckling.

Buckling was checked on the spar cap and aft panels. ANSYS simulations suggest that the baseline 5-MW design is very close (1% safety margin) to the buckling margin after applying the safety factors [13]. The results of this simplified methodology also predict that the baseline design is at the edge of buckling, but without application of the safety factor, thus no further safety factor was applied.

Like the ultimate strain calculation the constraint need only be applied a subset of the radial stations. The constraint is given as:

$$
\epsilon \leq \epsilon_b
\tag{9}
$$

2.1.6. Additional Rotor Constraints

For all designs, the rotor tip speed was constrained to be less than 80 m/s. This constraint was applied directly in the analysis. The maximum chord was constrained to be less than 5.3 m for consistency with road-based transportation constraints. The root bolt circle diameter was assumed to be 2.5% of the rotor diameter.

2.2. Tower Analysis

The towers optimized in this study were assumed to be steel tubular designs. Tower structural analysis was based on beam finite element analysis with 20 beam elements along the tower. It was assumed that the driving load cases for structural strain were the operational condition IEC DLC 1.3 with the extreme turbulence model (ETM), and the parked survival case IEC DLC 6.2. The ETM condition was approximated by computing rotor and tower loading at $V_{rated} + 3\sigma$ where the standard deviation for the ETM came from a class B site. For the survival case, it was assumed that one of the blades experienced a pitch failure and was thus unfeathered. The predicted static thrust from the rotor requires a dynamic amplification factor of 1.8–2.0 to fall within the range of dynamic thrust loadings from FAST simulations [21]. A factor of 1.8 was used in this analysis. Wind loading on the tower was estimated using a simple power-law profile, with drag coefficients for two-dimensional flow around a cylinder. Hoop stress was estimated using the methodology described by Eurocode [22]. The axial, shear, and hoop stress along the downwind side of the tower were combined into an equivalent von Mises stress. This stress was multiplied by a total safety factor of 1.485, and constrained to be less than the yield stress of 345 MPa. Like the rotor, the stress constraint was applied at a few subsections for efficiency.

Shell buckling was estimated using the methodology described by Eurocode [22] for a tapered cylinder with a safety factor of 1.35 for the loads, and 1.1 for buckling resistance. It was assumed the tower was reinforced every 30 m along the tower to decrease the effective buckling length. Global buckling was estimated using the methodology from Germanischer Lloyd [23] with the same safety factors.

Tower frequencies were constrained to be 10% higher than the rotor rotation frequency at rated conditions. In computing the frequency response of the tower, the rotor-nacelle assembly was treated as a rigid object offset from the tower top with mass properties supplied by the rotor and nacelle analyses.

A minimum tower diameter of 3.87 m was set to facilitate the connection of the nacelle and yaw-bearing. A maximum tower diameter of of 6.3 was set to facilitate road-based transportation[**]. To promote weldability of the tower sections, the

---

[||] Not all laminates in the blade are balanced and symmetric and so the zero entries in the matrix are actually nonzero. However, the magnitude of these terms is very small for the laminates studied here and are thus well approximated as specially orthotropic.

[**] While it is difficult to set a precise number on the upper bound of what is transportable, land-based tubular towers of this size have recently been developed [24]

diameter to thickness ratio was constrained to be greater than 120. For manufacturability the tower top diameter could not be smaller than 40% of the tower base diameter. The tower constraints are summarized as:

$$f_0 \geq 1.1\,\Omega_{max}$$
$$\eta_t\,\sigma_{VM1.3} \leq \sigma_y$$
$$\eta_t\,\sigma_{VM6.2} \leq \sigma_y$$
$$\text{shell buckling}_{1.3} \leq 1$$
$$\text{shell buckling}_{6.2} \leq 1 \quad (10)$$
$$\text{global buckling}_{1.3} \leq 1$$
$$\text{global buckling}_{6.2} \leq 1$$
$$d_{top} \geq 0.4\,d_{base}$$
$$d/t \geq 120$$

2.3. Nacelle

A new drivetrain model was developed to replace the former scaling model [25][††]. Some of the simpler drivetrain components used updated scaling relationships (bearings, yaw system, generator), while others used bottom-up physics models (bedplate, gearbox, low-speed shaft). For the purposes of facilitating gradient-based optimization in this study, each of the models was modified slightly in order to produce output that was continuously differentiable. This included fitting splines to look-up tables for bearing masses, moving internal sizing routines to constraints at the system-level optimization, and replacing any nondifferentiable functions (e.g., min, max, abs) with differentiable versions.

The bedplate was modeled with two I-beams. For simplicity the nondimensional proportions of each I-beam were kept constant, and the total height of each was used a design variable. The forward and aft I-beams were sized independently, each with constraints on bending stress and deflection. The low-speed shaft used a distortional energy failure theory. The design variables included the total shaft length, and the distance between bearings. Maximum deflections were applied as constraints. The gearbox had its own internal optimization, modifying the stage speed ratios to minimize its weight. The results of this optimization were smooth and simple enough to be kept internal to the system-level optimization. The constraints for the drivetrain are summarized as:

$$\sigma_{bedplate-fore} \leq \sigma_{max}$$
$$\sigma_{bedplate-aft} \leq \sigma_{max}$$
$$\delta_{bedplate-fore} \leq \delta_{max} \quad (11)$$
$$\delta_{bedplate-aft} \leq \delta_{max}$$
$$-\delta_{max} \geq \delta_{lss} \leq \delta_{max}$$

2.4. Cost Models

Critical to any optimization is the appropriate choice of an objective [11]. Using a goal of mass minimization or mass/AEP minimization would be inappropriate in this study. As will be explored in the results, the designs involve fundamental trade-offs primarily between energy capture, blade weight, and tower weight. Because the material cost per unit weight for composite rotor blades is much higher than the material cost per unit weight of steel towers (about 6:1 in our cost model), an objective based around mass would produce misleading results. The largest cost change in this application is in the turbine capital costs, driven by relative changes in blade and tower weight. Like other publicly available cost models, our capital cost model[‡‡] is simplistic as compared to those used by manufacturers. However, it has been calibrated with known project data in these size ranges, and is much better at capturing system trade-offs as compared to a mass-based optimization.

Reported values are expressed in terms of cost of energy using additional models for balance-of-station costs and operations and maintenance costs. The reported cost of energy values are not meant to represent actual costs, but are useful in comparing relative performance between designs. The resolution in the models is not high enough to distinguish between concepts with small differences in cost of energy, but cost differences of at least a couple percent can point towards concepts worth further exploration in detailed design.

[††] https://github.com/WISDEM/DriveSE
[‡‡] https://github.com/WISDEM/Turbine_CostsSE

2.5. Optimization

To reduce the number of design variables, distributed variables of interest were specified at a number of discrete locations along the blade and an Akima spline was used to define the variable in a continuous manner along the blade. All variables were defined on a normalized blade and subsequently made dimensional using the rotor hub and tip radii. Blade chord was specified at four points, with the location of max chord as an additional variable (Figure 2a). Twist was defined at four radial stations with a constant value across the cylindrical sections (Figure 2b). The spar cap thickness distribution used a spline across the outer portion of the blade with four control points and a single multiplier across the cylinder section (Figure 2c). Because of the complexity of the thickness distribution across the cylinder, rather than spline it directly, a multiplier was used to scale the baseline thickness distribution. For the aft panels, the reference model uses a step-like distribution of thickness, and that type of parameterization was preserved. A multiplier was also used across the cylinder section for the aft panels. For the outer portion of the blade, the thickness was defined as a constant value across four sections (Figure 2d). In this analysis, precurve was defined as the offset distance of the blade normal to the nominal blade reference axis (positive downwind). For cases with precurve, the precone angle was fixed at zero, otherwise the rotor diameter would be coupled to precurve. The reference blade has no precurve, but Figure 2e shows an example of the parameterization for a curved blade.

The nacelle variables included the bedplate I-beam height (fore and aft), and the lengths of the low-speed shaft, as discussed previously. The tower was parameterized as two linear tapered sections as shown in Figure 3. The waist location was normalized by the tower height. A summary of all the design variables is provided in Table II.

Optimizations were performed using SNOPT [26], a package for nonlinear optimization problems using the sequential programming method, and the optimizations were formulated in the OpenMDAO framework [27]. All constraints were scaled to be of order one for improved optimization convergence.

Some modules were broken up into smaller submodules to facilitate ease in deriving gradients. The total analysis consisted of a very large number of components. Often a simulation links only a handful of different codes together, but this analysis contained 102 modules, or components, each containing a separate analysis (e.g., blade aerodynamic performance, bedplate mass estimation, geometric splining, hub cost estimation, blade natural frequencies estimation, etc.). Analytic gradients were derived for all of the aerodynamic modules, cost modules, finance modules, and for some of the structural modules. Some of these gradients were derived by hand, while others were computed using automatic differentiation (Tapenade [28] and AlgoPy). An adjoint method was used to compute total derivatives for the rotor aerodynamics analysis (CCBlade). Of the 102 modules, we provided exact gradients for over 90% (92 components). Missing derivatives for the remaining 10 components, related to the structural analysis, were estimated using finite differencing. Total system derivatives were computed using the unified chain rule approach described by Martins and Hwang [29] as implemented in OpenMDAO. Because there were a larger number of constraints as compared to design variables, a forward method was used. OpenMDAO also computed the coupled aero/structural derivatives around the fixed point iteration used to solve blade deflection, and the coupled derivatives around the Brent solver used in the power curve module to find rated speed.

The benefits of using analytic derivatives, as opposed to finite differencing, for this problem are highlighted in a recent publication [5]. We found that despite care in deriving models with smooth output, global finite differencing was not good enough to converge many of the solutions. The analytic gradients derived in these models and a methodology to combine them into coupled system-level gradients was critical for this highly multidisciplinary analysis.
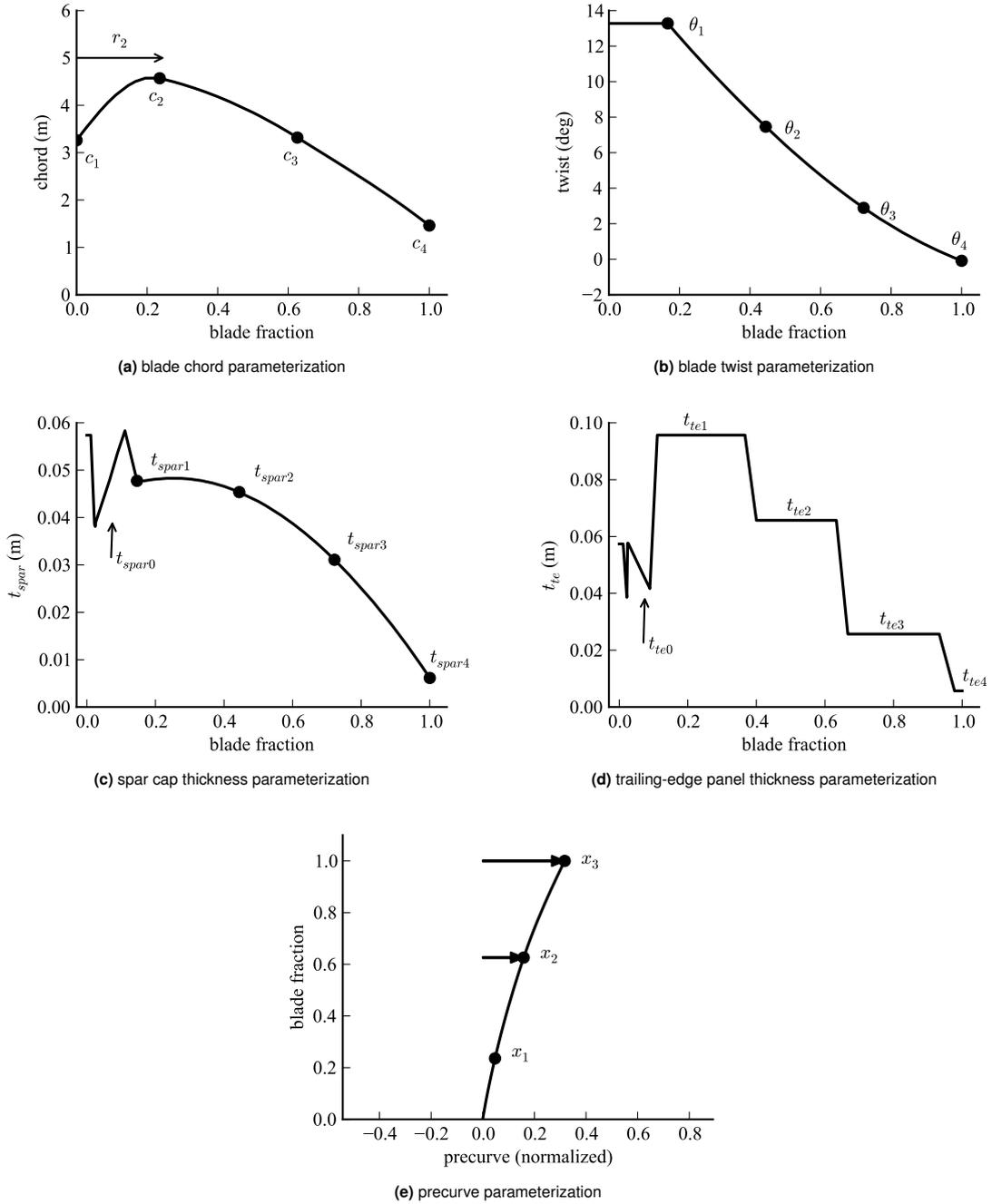
(a) blade chord parameterization

(b) blade twist parameterization

(c) spar cap thickness parameterization

(d) trailing-edge panel thickness parameterization

(e) precurve parameterization

Figure 2. Parameterization of some of the design variables used in defining the rotor blade geometry.
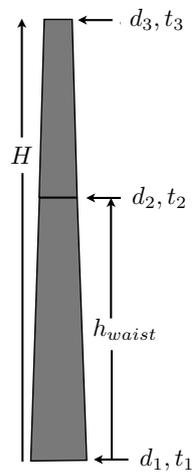
Figure 3. Tower parameterization.

Table II. Design variables used in optimization.

description	symbol	parameters
blade chord distribution	c	5
blade twist distribution	θ	4
spar cap thickness distribution	t_{spar}	5
aft panel thickness distribution	t_{aft}	5
blade precurve distribution	$x_{precurve}$	3
target tip-speed ratio in Region 2	λ_2	1
low-speed-shaft length	L_{shaft}	2
bedplate I-beam sizing	h_{beam}	2
tower height	H	1
tower waist location	h_{waist}	1
tower diameter	d	3
tower wall thickness	t_{wall}	3

3. DOWNWIND ROTORS

This section explores the performance of downwind rotors as compared to upwind rotors for three cases: 5-MW machines in Class I wind sites, 5-MW machines in Class III wind sites, and 7-MW machines in Class III wind sites. All designs used a precone angle of 2.5 degrees, a tilt angle of 5 degrees, and no precurve. For both upwind and downwind machines, the direction for tilt and precone was such that the separation distance between the blade tip and the tower increased. All designs were optimized for minimum cost of energy with the same set of constraints, except that the tower-strike deflection constraint was removed for downwind configurations.

Figure 4 compares the cost of energy (Fig. 4a), annual energy production (Fig. 4b), blade mass (Fig. 4c), and tower mass (Fig. 4d) as a function of rotor diameter for 5-MW machines in a Class I wind site. Each point in the curves represents an optimized design for a given diameter. For these design conditions, switching to a downwind design does not seem to provide any benefit. At the rotor diameter for minimum cost of energy (120 m), the downwind configurations does allow for a blade mass savings of 10% (Figure 4c). This blade mass savings was not as high as anticipated in some other conceptual studies. The reason for the relatively modest savings is that for Class I sites, the survival wind speed is a driving design condition and affects both the upwind and downwind designs in essentially the same way. Thus, alleviating the tower strike constraint does not provide as significant an advantage as one might expect. Additionally, while the lighter blades do reduce system costs, the designs are forced to utilize heavier towers (Figure 4d) which offsets the blade mass cost savings. A heavier tower is required because for downwind configurations the bending moment from the weight of the rotor-nacelle-assembly (RNA) is additive to the bending moment from the rotor thrust, whereas for upwind machines the RNA bending moment is in the opposite direction producing a reduced total tower top bending moment.
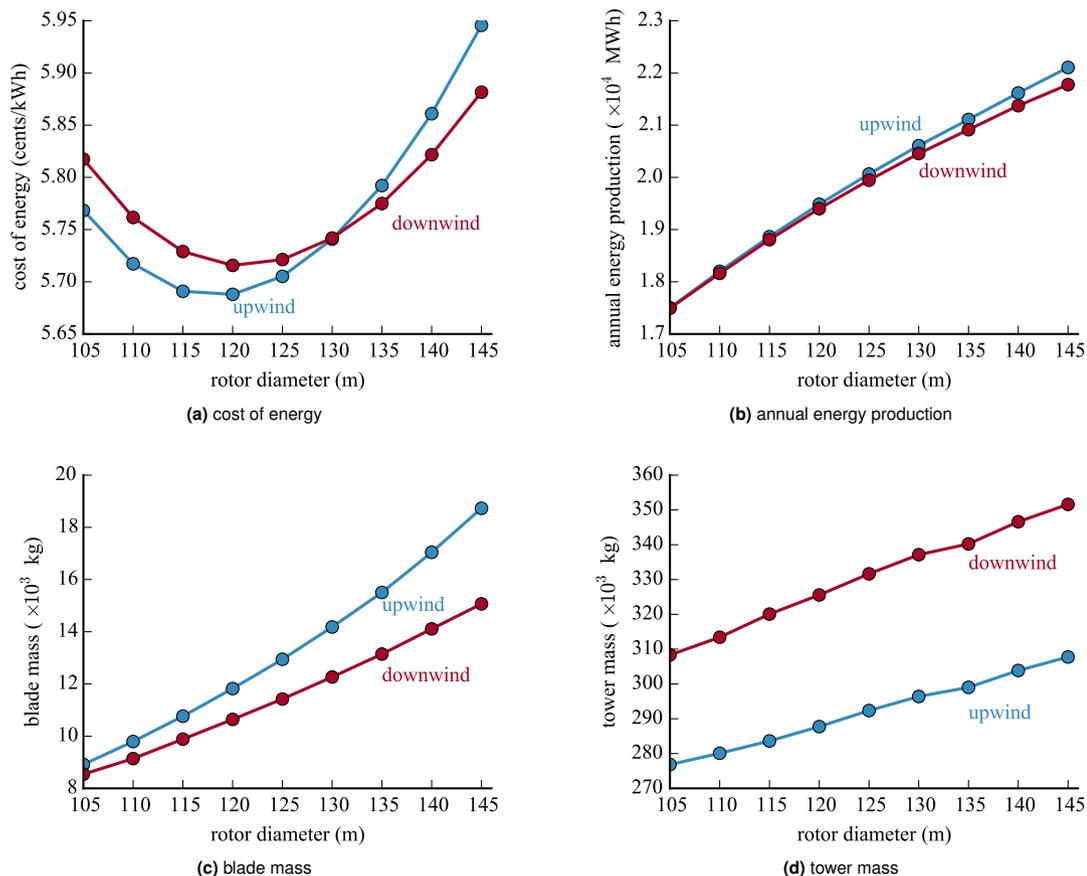

Figure 4. Variation in performance with rotor diameter for upwind and a downwind configurations (Class I wind, 5.0-MW rating).

The downwind designs also have slightly lower annual energy production because the operational loads deflect the blades away from a vertical position where energy production is maximized (the opposite occurs for the upwind designs to a limited extent depending on the tilt and precone angles), but the impact is slight (Figure 4b). The net result of the blade

mass reduction and tower mass increase is that the minimum cost of energy for the downwind configurations is slightly higher than the minimum cost of energy for the upwind configurations. For these design conditions, downwind machines do not appear to be advantageous.

The study was repeated for 5-MW designs in a Class III wind site. Large scale development potential exists for turbines optimized for low wind speed applications. Figure 5 shows the changes in cost of energy (Fig. 5a), annual energy production (Fig. 5b), blade mass (Fig. 5c), and tower mass (Fig. 5d) as a function of rotor diameter. For this lower wind speed class, the downwind configurations do show an advantage. The reduction in blade mass is much more significant. At a diameter of 145 m (near the minimum cost of energy), the downwind configurations utilize blades that are 30% lighter than the corresponding upwind design. Because the power rating is the same as the previous set of results, the maximum tip deflection in operational conditions is similar. However, for this lower wind speed site, the survival wind speeds are much lower and the operational tower strike constraint becomes a much more dominant constraint. Thus, the benefit to switching to a downwind configuration is more pronounced.

Like the previous case, the disadvantages of the downwind configuration still lead to a heavier tower (17% heavier), and a reduced AEP (1% lower). Still, the minimum cost of energy downwind design has a 1.5% lower cost of energy than the minimum cost of energy upwind design. The optimal downwind design also occurs at a larger diameter than does the optimum upwind design. Conceptual studies generally cite the large blade mass savings, and indeed a large blade mass savings of 30% was realized. However, once accounting for the increase in tower mass and a small drop in energy production, the cost of energy savings is much more modest. The resolution in the cost model in this conceptual design study is not such that a 1.5% margin could be called a definitive advantage, however it does suggest that downwind turbines for Class III sites may be worth further exploration in detailed design.
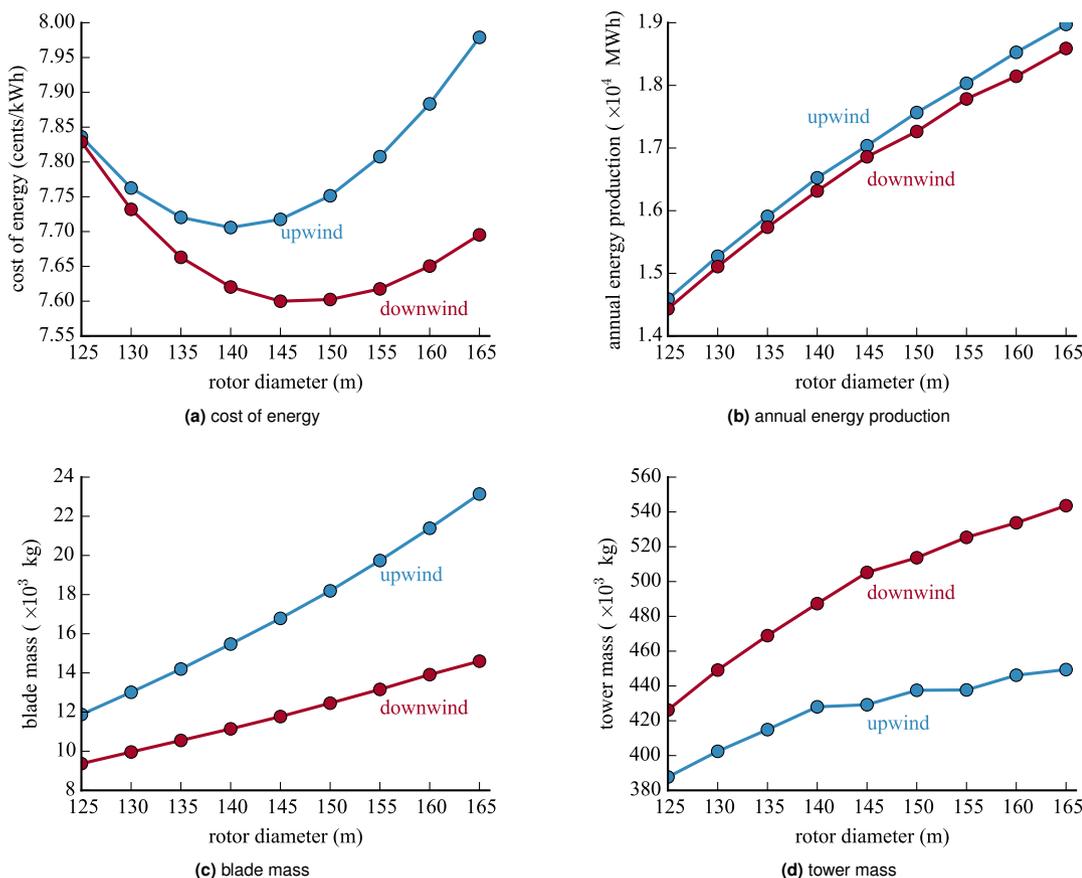

Figure 5. Variation in performance with rotor diameter for upwind and a downwind configurations (Class III wind, 5.0-MW rating).

The last case explores larger 7-MW designs. Figure 6 shows the changes in cost of energy, annual energy production, blade mass, and tower mass as a function of rotor diameter. The benefits are similar to the 5-MW Class III case. For a given wind class, one would expect that turbines with higher power ratings would benefit to a larger degree from a downwind
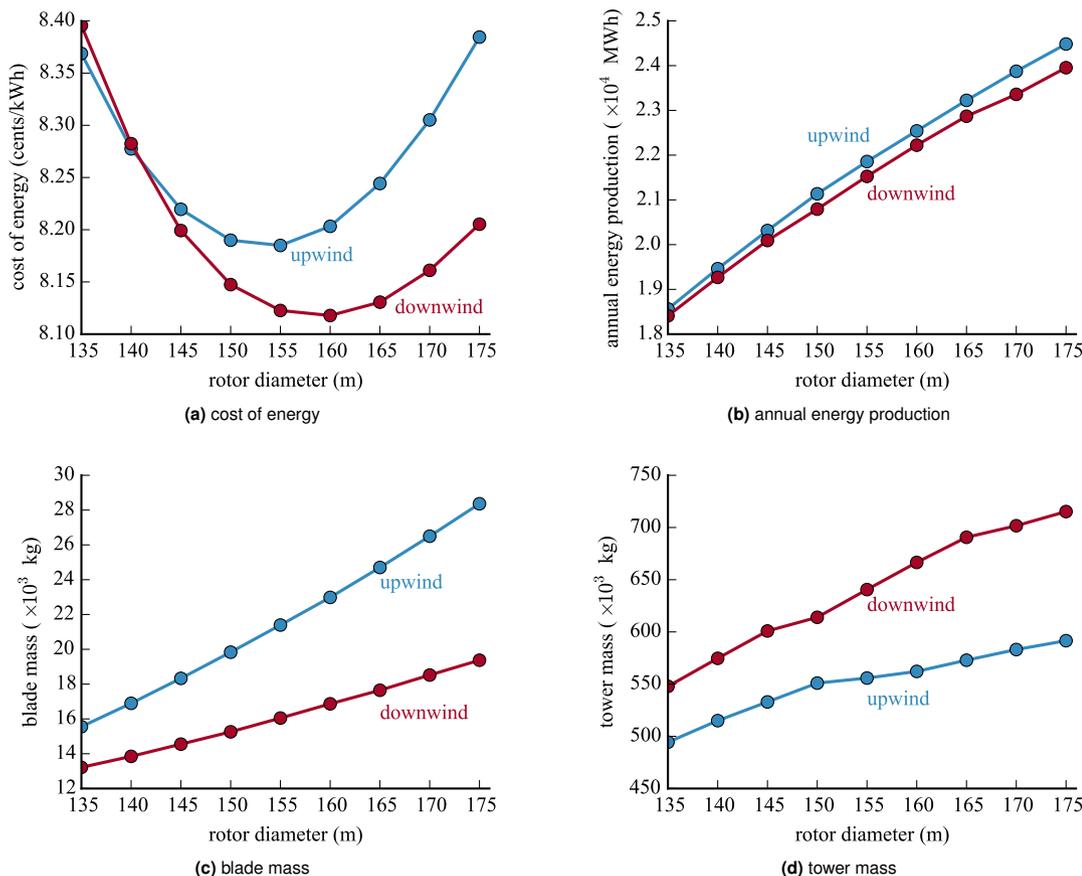
Figure 6. Variation in performance with rotor diameter for upwind and a downwind configurations (Class IIII wind, 7-MW rating).

configuration. A larger machine rating translates into larger maximum tip deflections, increasing the potential benefit of alleviating the tower-strike constraint. However, the design freedom was highly limited for these larger machines. While the total thickness of the laminate stacks was optimized, the same layup sequence and nondimensional airfoil profile that was designed for the 5-MW reference model was used. Furthermore, only tubular steels towers were explored within the scope of this study. More efficient turbines are likely to be found by utilizing hybrid or truss-style towers, and incorporating additional carbon in the blades. The tower base diameter was a severely restrictive constraint for these designs given the large power rating and tubular tower concept. Regardless, significant savings in blade mass were apparent from switching to a downwind configuration for these Class III wind sites. Whether or not that translates into significant system cost savings depends on detailed design decisions for downwind configurations and how they impact tower mass, performance losses from blade flexibility, and performance losses and increased fatigue damage from operating in a tower shadow.

4. PRECURVED DOWNWIND BLADES

Conceptual studies suggest that even larger blade mass reductions are possible by precurving the blade downwind for downwind rotors [30]. By aligning the blades in the direction of the local combined loading (aerodynamic, weight, centrifugal) at rated speed, the bending loads are significantly reduced and thus a lighter structure is possible. We compared a straight blade with 0 degrees precone, with a blade precurved to align with the load direction at rated speed (an average of the aligned precurve for $0°$ and $180°$ azimuth). The precurved blade was lengthened in order to maintain a constant diameter. No additional sizing was performed for this comparison. The reference axis for both blades can be seen in Figure 7.

Table III summarizes some of the major changes in the design criteria. The data shows that indeed the strain at the operational condition was decreased dramatically (37% reduction), however the survival loading condition was more
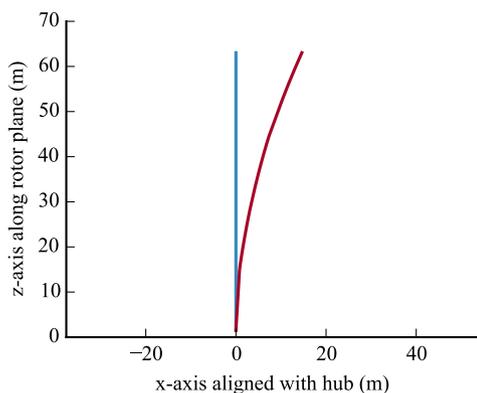
Figure 7. Profile of downwind blade with fixed precone and highly curved blade based on minimizing bending-loads at rated conditions. The wind direction is left to right.

Table III. Comparison of straight blade and curved blade concept.

	straight blade	curved blade
rated max strain (μstrain)	1,336	841
survival max strain (μstrain)	3,001	2,872
1st flap frequency (Hz)	0.961	0.848
1st edge frequency (Hz)	1.15	1.08
AEP (MWh)	19,560	18,802

critical for blade sizing and the decrease in strain at that condition was very modest (4% reduction). The reason for the diminished impact, is that at survival wind conditions the local force angle is primarily downwind in the thrust direction and the benefits of precurvature are far less dramatic. The curvature of the blades creates a longer blade, which results in significantly lower natural frequencies. Resonance avoidance of the blades is often a driving constraint which would further reduce the advantage of the longer blade.

The precurved design also resulted in a 4% loss in annual energy production, however this drop in power prediction may be overly conservative. As noted in the future work discussion (Section 5), work by Crawford [31] suggests that BEM methods underpredict power performance for highly coned downwind machines. Still, it is not expected that a downwind curved blade would increase power production. Even ignoring the power production changes, the benefits for high downwind curvature appear to be minimal. The strain reduction at survival wind conditions is small, and the decreased frequency margin would require additional blade stiffness, offsetting mass savings from the decreased maximum strain. The very features that make curved downwind blades advantageous structurally, namely decreased loading and high flexibility, are generally disadvantageous aerodynamically. Downwind precurvature could be highly beneficial if the structural response of the blades could be tailored to be stiff and oriented perpendicular to the wind around rated speed, but respond flexibly and shed loads near the high-speed survival wind conditions.

Extending the analysis of a preselected curvature, a final case was examined where precurvature was added as a design variable to the optimization. The blade was prevented from curving beyond the blade root in lieu of a tip-strike thrust reversal constraint, and the maximum precurvature was limited to 6.3 m for transportation reasons. This case study used a 5-MW turbine at a Class III site, with an objective of minimizing cost of energy. The diameter was set at 145 m, which was approximately the optimal diameter for this configuration (Figure 5a). The optimized shape of the blade both unloaded, and at $0.7\,V_{rated}$ is shown in Figure 8. The resulting optimized blade for the downwind machine was actually precurved upwind, in the opposite direction of the blades discussed earlier in this section. This type of curvature was favored because under load the blade is close to perpendicularly aligned near rated speed for increased power capture. Adding precurvature in the optimization decreased the cost of energy by an additional 2.5% beyond the corresponding design in Figure 5a (an upwind design showed a similar savings in cost of energy through optimized precurvature).

While detailed design studies are needed to more completely assess precurvature impacts, this type of upwind curvature is especially beneficial for upwind configurations. For upwind configurations the increase in power would be similar to the downwind case, but for an upwind machine the tower-strike margin would increase rather than decrease. This type of upwind curvature is observed in most modern turbine designs.
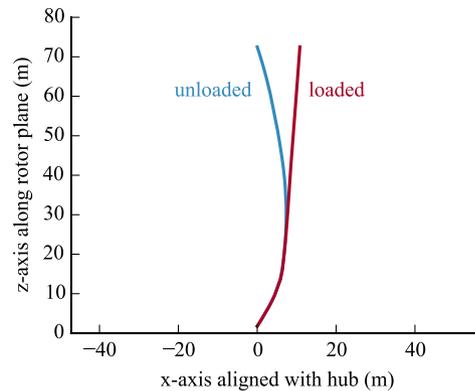
Figure 8. A downwind rotor blade with optimized precurvature shown both unloaded and loaded.

5. CONCLUSION

This research has focused on comparing upwind and downwind rotors for land-based turbines. Blade element momentum theory was used to model aerodynamics, and classical laminate theory with beam finite element analysis was used to model the structures. Nacelle, tower, and cost models were included to allow for assessment of cost of energy. Analytic gradients were derived for 90% of the 102 components in the system analysis to facilitate efficient and scalable optimization.

Traditional upwind designs become less efficient at larger rotor diameters and larger power ratings where the tower-strike constraint forces the blades to be very stiff. While upwind configurations still appear to be optimal for most of today's designs, as rotors become larger, machine ratings increase, and lower wind speed sites are more heavily utilized, downwind turbines provide some potential benefits. The results of the studies in this paper suggest that for Class III wind sites, significant savings in the structural mass of the blade are possible (around 25-30%). However, these benefits are somewhat offset by larger tower masses required for downwind configurations because the bending moment from the rotor-nacelle-assembly weight becomes additive to that of the bending moments from the rotor thrust. Additionally, the deflection of the blade under operational loading tends to decrease annual energy production. Still, modest savings in cost of energy of around 1-2% may be possible.

Large downwind precurvature was not seen to be beneficial within the parameters of this study. The large curvature did indeed decrease strain at operational conditions, but also decreased power production, margin against frequency constraints, and was less effective in reducing strain during survival load conditions. Optimally curved blades were actually curved upwind in order to maximize power capture. Downwind precurvature could be useful if the structural laminate was specifically optimized to provide stiff response near rated speed for high power capture, but responded flexibly at higher survival wind speeds.

CFD analysis by Crawford suggests that BEM methods underpredict power performance for highly coned downwind machines [31]. Additionally, his work provides some updates to the BEM method that allow for better predictions for coned rotors. Those corrections were not incorporated in these studies, primarily because of our focus on analytic gradients at the system-level, but should be considered in future work. The results of this paper yielded only relatively small blade curvature, but a better power-performance model might push the designs towards higher curvature than explored here.

Downwind rotors show potential for reduced cost of energy, but further research is needed to study the dynamic effects of the more flexible downwind blades. Only three-bladed concepts were explored in this study to allow more direct comparison to traditional upwind designs, but even greater mass reductions may be possible through downwind two-bladed designs. Further benefits would also result from airfoil shape optimization and composite laminate sequence tailoring. Additional studies are needed to quantify the fatigue and acoustic impact of tower shadow on the designs, and explore concepts to alleviate the corresponding increase in fatigue. Improvements in the cost models and plant models are needed to capture other potential downwind turbine benefits such as simpler yaw systems and increased power capture in complex terrains. Penalties from the tower top bending moment could be reduced through more detailed drivetrain/nacelle design by shifting the center of mass closer to the tower top. These and other improvements should be explored to better quantify the potential benefits and limitations of downwind turbines at utility-scale.

ACKNOWLEDGMENTS

REFERENCES

1. Maki K, Sbragio R, Vlahopoulos N. System design of a wind turbine using a multi-level optimization approach. *Renewable Energy* jul 2012; **43**:101–110, doi:10.1016/j.renene.2011.11.027. URL http://dx.doi.org/10.1016/j.renene.2011.11.027.

2. Diveux T, Sebastian P, Bernard D, Puiggali JR, Grandidier JY. Horizontal axis wind turbine systems: optimization using genetic algorithms. *Wind Energy* oct 2001; **4**(4):151–171, doi:10.1002/we.51. URL http://dx.doi.org/10.1002/we.51.

3. Lyu Z, Xu Z, Martins JRRA. Benchmarking optimization algorithms for wing aerodynamic design optimization. *The Eighth International Conference on Computational Fluid Dynamics*, Chengdu, Sichuan, China, 2014.

4. Fleming P, Ning A, Gebraad P, Dykes K. Wind plant system engineering through optimization of layout and yaw control. *Wind Energy* Mar 2015; doi:10.1002/we.1836.

5. Gray J, Hearn T, Moore K, Hwang J, Martins J, Ning A. Automatic evaluation of multidisciplinary derivatives using a graph-based problem formulation in OpenMDAO. *15th AIAA/ISSMO Multidisciplinary Analysis and Optimization Conference*, Atlanta, GA, 2014, doi:10.2514/6.2014-2042.

6. Janajreh I, Qudaih R, Talab I, Ghenai C. Aerodynamic flow simulation of wind turbine: Downwind versus upwind configuration. *Energy Conversion and Management* Aug 2010; **51**(8):1656–1663, doi:10.1016/j.enconman.2009.12.013. URL http://dx.doi.org/10.1016/j.enconman.2009.12.013.

7. Reiso M, Muskulus M. The simultaneous effect of a fairing tower and increased blade flexibility on a downwind mounted rotor. *Journal of Renewable and Sustainable Energy* 2013; **5**(3):033 106, doi:10.1063/1.4803749. URL http://dx.doi.org/10.1063/1.4803749.

8. Yoshida S. Performance of downwind turbines in complex terrains. *Wind Engineering* Dec 2006; **30**(6):487–501, doi:10.1260/030952406779994169. URL http://dx.doi.org/10.1260/030952406779994169.

9. Reiso M, Moe G. Blade response on offshore bottom fixed wind turbines with down-wind rotors. *29th International Conference on Ocean, Offshore and Arctic Engineering: Volume 3*, ASME, 2010, doi:10.1115/omae2010-20586. URL http://dx.doi.org/10.1115/omae2010-20586.

10. Wind turbines part 1: Design requirements. *Technical Report IEC 61400-1*, International Electrotechnical Commission 2005.

11. Ning A, Damiani R, Moriarty P. Objectives and constraints for wind turbine optimization. *Journal of Solar Energy Engineering* Nov 2014; **136**(4), doi:10.1115/1.4027693.

12. Ning A, Dykes K. Understanding the benefits and limitations of increasing maximum rotor tip speed for utility-scale wind turbines. *Journal of Physics: Conference Series* Jun 2014; **524**(012087), doi:10.1088/1742-6596/524/1/012087.

13. Resor BR. Definition of a 5MW/61.5m wind turbine blade reference model. *SAND2013-2569*, Sandia National Laboratories Apr 2013.

14. Fingersh LJ, Hand MM, Laxson aS. Wind turbine design cost and scaling model. *NREL/TP-500-40566*, National Renewable Energy Laboratory, Golden, CO Dec 2006.

15. Ning A. A simple solution method for the blade element momentum equations with guaranteed convergence. *Wind Energy* Sep 2014; **17**(9):1327–1345, doi:10.1002/we.1636. URL http://dx.doi.org/10.1002/we.1636.

16. Jonkman J, Butterfield S, Musial W, Scott G. Definition of a 5-MW reference wind turbine for offshore system development. *NREL/TP-500-38060*, National Renewable Energy Laboratory, Golden, CO Feb 2009.

17. Larwood SM. Dynamic analysis tool development for advanced geometry wind turbine blades. PhD Thesis, University of California Davis 2009.

18. Guideline for the certification of wind turbines. *Technical Report*, GL Renewables Certification 2010.

19. Halpin JC. *Primer on Composite Materials Analysis*. 2nd edn., Technomic, 1992.

20. Johnson A. *Handbook of Polymer Composites for Engineers*, chap. Structural Component Design Techniques. Woodhead Publishing, 1994.

21. Jonkman JM. Dynamics modeling and loads analysis of an offshore floating wind turbine. *Technical Report NREL/TP-500-41958*, National Renewable Energy Laboratory Dec 2007, doi:10.2172/921803. URL http://dx.

doi.org/10.2172/921803.

22. European Committee for Standardisation. Eurocode 3: Design of steel structures—part 1-6: General rules—supplementary rules for the shell structures. *EN 1993-1-6: 20xx* 1993.

23. Guideline for the certification of offshore wind turbines. *Technical Report IV – Part 2, Chapter 6*, Germanischer Lloyd 2005.

24. Franco MD. Oems building bigger, better mousetraps. *North American Windpower* May 2014; **11**(5).

25. Guo Y, King R, Parsons T, Dykes K. A wind turbine drivetrain sizing and optimization model set. 2015. (forthcoming).

26. Gill PE, Murray W, Saunders Ma. SNOPT: An SQP algorithm for large-scale constrained optimization. *SIAM review* 2005; **47**(1):99–131.

27. Gray J, Moore KT, Hearn TA, Naylor BA. Standard platform for benchmarking multidisciplinary design analysis and optimization architectures. *AIAA Journal* Feb 2013; **51**(10):2380–2394, doi:10.2514/1.J052160. URL http://dx.doi.org/10.2514/1.J052160.

28. Hascoët L, Pascual V. The tapenade automatic differentiation tool: principles, model, and specification. *ACM Transactions On Mathematical Software* 2013; **39**(3), doi:10.1145/2450153.2450158.

29. Martins JRRA, Hwang JT. Review and unification of methods for computing derivatives of multidisciplinary computational models. *AIAA Journal* Oct 2013; **51**(11):2582–2599, doi:10.2514/1.J052184.

30. Loth E, Steele A, Ichter B, Selig M, Moriarty P. Segmented ultralight pre-aligned rotor for extreme-scale wind turbines. *50th AIAA Aerospace Sciences Meeting including the New Horizons Forum and Aerospace Exposition*, 2012, doi:10.2514/6.2012-1290.

31. Crawford C. Re-examining the precepts of the blade element momentum theory for coning rotors. *Wind Energy* 2006; **9**(5):457–478, doi:10.1002/we.197. URL http://dx.doi.org/10.1002/we.197.